Structure and Dynamics of Metallic and Carburized Catalytic Ni Nanoparticles: Effects on Growth of Single-Walled Carbon Nanotubes

Jose L. Gómez-Ballesteros and Perla B. Balbuena*
Department of Chemical Engineering
Texas A&M University, College Station, TX 77843
*e-mail: balbuena@tamu.edu

Abstract

Understanding the evolution of the catalyst structure and interactions with the nascent nanotube at typical chemical vapor deposition (CVD) conditions for the synthesis of single-walled carbon nanotubes is an essential step to discover a way to guide growth toward desired chiralities. We use density functional theory (DFT) and ab initio molecular dynamics (AIMD) simulations on model metallic and carburized Ni clusters to explore changes in the fundamental features of the nanocatalyst: geometric and electronic structure, dynamics and stability of the carburized nanocatalyst, and interactions with nascent nanotube caps at two different temperatures (750 and 1000 K) and different carbon composition ratios. This allows us to gain insight about the evolution of these aspects during the pre-growth and growth stages of CVD synthesis of single-walled carbon nanotubes and their implications for reactivity and control of the nanotube structure.

Introduction

A significant and sustained interest in finding ways to synthesize nanomaterials has emerged a couple of decades ago. Motivation for this was nourished by predictions of materials with extraordinary properties conferred by their nanometric dimensions. Among the ample variety of nano-sized novel materials that continue to cause fascination, carbon nanotubes maintain interest as new exciting applications emerge, and efforts to produce them in a selective and efficient manner continue to increase[1]. Potential uses of single-walled carbon nanotubes (SWCNTs) range from nanoelectronic devices such as electron field transistors[2], to biomedical[3], separations[4], electrochemistry[5] and other innovative energy-related applications[6]. The attractiveness of SWCNTs for these and other emerging applications is derived from their outstanding properties including excellent thermal conductivity[7], electron mobility[8], electron transfer in electrodes[9], optical properties[10] and mechanical stability[11].

A number of synthesis techniques have been developed to fabricate SWCNTs at low cost and large-scale[12]. However, the lack of control of the nanotube structure (and associated chirality) remains to be one of the main obstacles for the selective synthesis of SWCNTs. Structural features such as diameter, length, defect density, and chiral angle are fundamental to determine the suitability of SWCNTs for each particular application due to the strong structural dependence

of their properties[13]. Despite the existence of complex separation techniques that can achieve a high degree of purity of SWCNT with specific features[14-16], developing methodologies to selectively produce SWCNT stays in the spotlight of researchers as a more efficient and economically viable option.

Catalytic chemical vapor deposition (CVD) is currently one of the most commonly used methods for the synthesis of SWCNTs. Some of its main advantages are a relatively low cost and high degree of control and scalability[1]. A typical CVD scheme operates at temperatures ranging from 600 to 1300 K, and pressure between 1 and 5 atmospheres. Supported or floating transition metal nanoparticles in a gas phase reactor are used as catalysts and hydrocarbons, ethanol, methanol, CO_2 or CO are usually the carbon sources[17,18]. Experimental[19,20] and theoretical studies[21-24] aiming to reveal the growth mechanisms at the atomic scale have allowed the elucidation of important features of the catalyst and the nanotube during the nucleation and growth stages and continue to bring questions that motivate further research into each aspect. One example in particular is the observation of SWCNT growth on pure transition metal catalysts[25] and on carbide nanocatalysts[26,27], raising questions such as what is the role of C atoms dissolved in the nanoparticle? How can they affect the structure and activity of the catalyst? And how does the structure of the catalyst influence the type of carbon nanostructure grown on its surface?

A fundamental aspect that may be crucial to determine the final nanotube structure during CVD is the correlation between the nascent nanotube and the structure of the nanocatalyst. Among proposed growth mechanisms, a *template effect* in which the nucleation process of the nascent cap structure is guided by the structure of the supported nanocatalyst has been predicted and observed[24,28,29]. The opposite case where the nanocatalyst accommodates its shape to the growing carbon nanostructure has also been observed and is known as *inverse template effect*[30]. The second case is more likely to be observed during synthesis using a floating catalyst[31-33]. Current experimental techniques such as electron scanning microscopy have allowed in situ atomic scale observations, providing evidence of the influence that the nanoparticle structure can have on the nascent nanotube[29,34]. Such observations can be further examined and interpreted with the use of quantum mechanical calculations. Computational tools such as density functional theory (DFT) and ab initio molecular dynamics (AIMD) are helpful providing relevant information to elucidate the key aspects of the catalyst that may be determinant of the nanotube structure. Consequently, exploring and understanding the structure and chemical nature of the nanocatalyst becomes a required step toward elucidating growth mechanisms and using them as tools to devise control strategies over the structure of SWCNTs.

Ni, Co, and Fe are the most common catalysts in SWCNT synthesis. DFT calculations of Ni nanoparticles in contact with model nanotubes have been previously studied and reported in the literature. Borjesson et al. investigated the effect of the $Ni_{55}C_x$ carbide composition on SWCNTs growth by estimating the binding energies between SWCNTs with specific chiralities (namely (3,3), (5,5), (9,1) and (10,0)) and both Ni and Ni carbide particles. They concluded that

nanotubes interact more strongly with the pure metal than with the carbide; however the difference was reported as small compared with the total adhesion energies[35]. Wang et al. also studied adhesion energies, chemical potential and charge distribution between Ni_{55} clusters and selected nanotube caps with chiralities (5,5), (6,5) and (9,0). The energetics of the different carbon structures in contact with the nanoparticle showed small differences and were characterized by electron transfers between the nanoparticle and the nanotube[36].
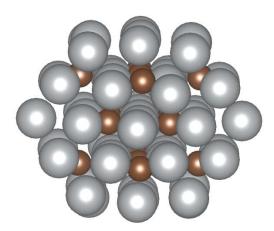
The dynamics and stability of a carburized nanocatalyst at the synthesis temperature, its local composition, shape, electronic structure, and interactions with nascent nanotube caps are the focus of the present work. Although the dynamic evolution of the catalyst and the nanotube has been studied in the past using reactive classical molecular dynamics providing a step-by-step picture of the catalytic process, diffusion in the nanoparticle, and incorporation into the growing nanotube of the precursor carbon [37,38], it is important to gain further insights of the effects of electronic distribution without the bias imposed by effective force fields. Here we use AIMD to study the dynamics of a carburized Ni nanoparticle at typical CVD synthesis conditions and the same nanoparticle in contact with model nanotube caps resembling the early stages of nanotube growth. Because the extension of the simulated time frame is limited and phenomena such as the incorporation of C atoms to the nanotube rim are not included, this study resembles growth in the limit of low pressure of precursor gas. Comparisons between the pure metallic particle and the carburized particle help to elucidate the interactions of these catalysts with the growing carbon nanotube.

Computational Methods

We use spin-polarized DFT calculations with the Perdew-Burke-Ernzerhof exchange-correlation functional[39] implemented in the Vienna ab-initio simulation package (VASP)[40-44]. The electron-ion core interactions are treated with the projector augmented wave (PAW) pseudo-potentials[45,46] and the valence charge density with a plane wave basis set with a cutoff energy of 400 eV. The geometry relaxations were performed using the conjugate gradient algorithm with an energy stopping criterion of 10^{-3} eV, and for the electronic self-consistent loop 10^{-4} eV was employed. A Gaussian smearing with a 0.05 eV width was used. AIMD simulations were performed using the NVT ensemble at 750 and 1000 K with the Nosé thermostat and a time step of 1 fs. A Γ-point Brillouin zone sampling for integration in the reciprocal space was used for energy relaxations and in AIMD simulations. Estimation of atomic charges was performed using the Bader charge analysis scheme, in which the electronic charge density enclosed within an atom defined by zero flux surfaces corresponds to the total electronic charge of said atom[47,48]. The base model in our simulations is a 55-atom Ni nanoparticle in a cubic box with side length of 3 nm, allowing sufficient space to avoid interactions with periodic images in any direction. Modifications to our model include the successive addition of C atoms into octahedral sites to resemble carbon dissolution and carbide formation, followed by attachment of chiral nanotube caps over the nanocatalyst structure.

Our initial model consists of a 55-atom unsupported Ni nanoparticle constructed using Materials Studio®[49]. The nanostructure was built taking a Ni face-centered cubic (fcc) crystal as a base. After relaxation of the initial structure, a progressive addition of C atoms into octahedral sites within the nanoparticle structure was performed. For each C addition the nanoparticle structure was allowed to relax. C atoms were added until saturation of the octahedral sites inside the nanoparticle was reached while maintaining a stable structure (Figure 1). The energy of interaction of the individual carbon atoms was estimated by subtracting the sum of energies of the nanoparticle without carbon (E_{Ni55}) and number of C atoms (n) times the energy of an isolated carbon (E_C) atom from the energy of the system (E_{Ni55Cn}). The result was normalized dividing by the number of carbon atoms added.
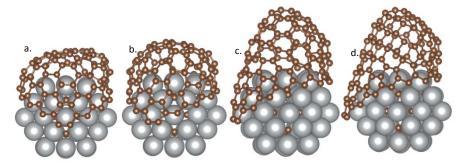
$$E_{int} = \frac{E_{Ni55Cn} - (E_{Ni55} + n \cdot E_C)}{n} \qquad (1)$$

Figure 1. Side view of the structure of $Ni_{55}C_{14}$ after locating C atoms in the inner octahedral interstitial sites of a Ni_{55} unsupported cluster. Gray and brown spheres represent Ni and C atoms, respectively.

In order to study the interactions of the nickel nanoparticle and the carbon atoms dissolved within its structure with the nascent nanotube, model nanotube caps were constructed using the software CaGE[50]. Nanotube caps were built taking into account the isolated pentagon rule, according to which the stability of the cap is favored when the six pentagons needed in the structure are isolated from one another[51]. Figure 2 illustrates the model carburized nanoparticle in contact with the nanotube caps. Four model nanotube caps were considered for nanotubes with chiral indexes (8,7), (9,6), (11,5), and (13,0) in representation of chiral nanotubes with semiconducting (Figure 2a) and metallic character (Figure 2b and c) and zigzag nanotubes with semiconducting character (Figure 2d). The cap indexes were selected to obtain nanotubes with a

diameter slightly larger than the nanoparticle diameter. The caps were placed in contact with relaxed structures of $Ni_{55}C_{14}$ nanoparticles.

Figure 2. Side view of the structure of the carburized $Ni_{55}C_{14}$ in contact with four different nanotube cap models with chiral indexes (n,m): a. (8,7), b. (9,6), c. (11,5) and d.(13,0). Gray and brown spheres represent Ni and C atoms, respectively.

The dynamics of the carbon atoms inside the unsupported Ni nanoparticle at two different temperatures, 750 K and 1000 K, was studied during 8 ps for two different compositions $Ni_{55}C_{10}$ and $Ni_{55}C_{14}$ using AIMD simulations. Further AIMD for the $Ni_{55}C_{14}$ nanoparticles in contact with four different model nanotube caps was carried out for a simulation time of 3 ps. The individual trajectories of carbon were followed to obtain useful information about the dynamic evolution of the nanocatalyst structure, the influence of the nascent nanotube and the occurrence of carbon association.

Results and Discussion

Energetics of carbon dissolution and evolution of atomic interactions. Table 1 shows that for each successive addition of C atoms to the Ni nanoparticle, the energy of the carburized particle is lower than the sum of the energies of the Ni nanoparticle and C atoms separately. Thus, the incorporation of C atoms into the nanoparticle structure is thermodynamically favorable, as expected for transition metals capable of dissolving carbon. Across additions the energy of interaction is consistent (mean=-6.49, standard deviation=0.12)

Table 1. Energy of the system and energy of interaction for each successive addition of carbon into the Ni nanoparticle as defined in equation (1).

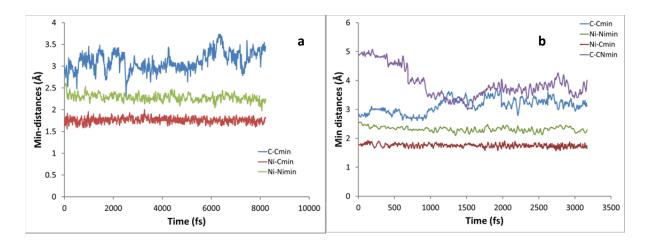| #C atoms	0	1	2	4	6	8	10	14
E_interaction(eV)	0.0	-6.48	-6.40	-6.57	-6.59	-6.57	-6.55	-6.27

The composition of the particle once the octahedral sites were occupied without deformation of the particle shape and structure was $Ni_{3.92}C$. This C concentration is lower than those of stable or

metastable carbides such as Ni_3C and Ni_2C. The ability of a Ni nanoparticle to dissolve C is dependent on its size and the conditions it is exposed to (temperature and C chemical potential). Systematic analyses of the stability of carburized Ni nanoparticles have been performed using computational tools such as tight binding and Monte Carlo simulations[52,53] reporting that carbon solubility tends to increase with: a) decreasing particle size, b) increasing temperature, c) increasing chemical potential (pressure of precursor gas). Similar behavior has also been observed for other transition metals[54]. Generally, a nanoparticle has a much higher limit of C dissolution than a bulk metal has, which in turn affects the melting temperature by decreasing it at growth conditions[54]. Thus, it is expected for the particle morphology to change dramatically from that shown in Figure 1. This has been clearly observed using classical molecular dynamics simulations at the CVD temperatures (~ 1000 K)[37,38] and *in situ* experimental techniques such as environmental transmission electron microscopy (ETEM) imaging of SWCNT growth on Ni and transition metals, in which structural fluctuations and reshaping effects are present with[55] and without[56] (negligible) carbon dissolution Though carbide phases have been identified in nanoparticles at growth conditions[34,57], there is still a debate regarding the formation and stability of carbide or surface carbide during the SWCNT process. Here minimum distances between C-C, Ni-C and Ni-Ni atoms were monitored throughout the AIMD simulations to observe variations in the nanoparticle structure and evaluate whether association among C atoms dissolved in the nanoparticle would be possible.

Figure 3a illustrates the minimum distances between Ni and C atoms in the carburized Ni nanoparticle of composition $Ni_{55}C_{14}$ at 1000 K. Ni-Ni distances were observed to be maintained about an average value of 2.27 Å, which is in fair agreement with typical Ni interlayer distances in Ni carbides[58,59]. Ni-C minimum distances show little variation around an average value of 1.76, in agreement also with distances found in Ni carbides[58,59]. C-C minimum distances were found to be kept out of range for C-C bond formation, with a lowest minimum distance of 2.29 Å. Therefore C-C association inside the nanoparticle is not found. The average minimum C-C distance is 3.11 Å with a standard deviation of 0.22 Å, showing greater variability with respect to Ni-C and C-C.

Higher variation of the C-C minimum distance accompanied by a gradual increase in its value is a reflection of the dynamics of C atoms migrating from their original octahedral positions towards the subsurface of the nanoparticle. Such migration process is further illustrated in the analyses of individual atom-pair distances followed throughout the simulation time. The effect of varying nanoparticle composition and temperature was found to be practically insignificant for Ni-Ni and Ni-C minimum distances. Variations in C-C minimum distances for different compositions and temperature can be attributed to statistical variability within each set of conditions.

Figure 3. Monitoring of minimum distances found during the simulated time between Ni-Ni, Ni-C, C-C and C-CN, where C-C refers to distances between C atoms inside the nanoparticle and C-CN are distances between C in the nanotube cap rim and C atoms dissolved in the nanoparticle. a) $Ni_{55}C_{14}$ at 1000 K and b) $Ni_{55}C_{14}$ in contact with the nanotube cap of indexes (8,7) at 750 K.

Interactions between a carbon cap and the carbide nanoparticle. Figure 3b shows the dynamic evolution of the minimum distances between Ni and C atoms for the carburized nanoparticle having a (8,7) nanotube cap attached to its surface (shown in Figure 2a). Ni-Ni and Ni-C minimum distances showed little variation with respect to the type of cap in contact with the nanoparticle, with average distances of 2.33 Å and 1.79 Å respectively. These values remained almost constant throughout the simulation time. The C-C minimum distances increased as the simulation progressed as a result of the bulk diffusion of the C atoms inside the nanoparticle and migration toward the subsurface. In Figure 3b we analyze the minimum distances between C atoms in the rim of the nanotube cap and the C atoms inside the nanoparticle (named C-CN). In all four cases of caps studied, minimum C-CN distances were out of range for bonding interactions between C atoms during the extension of the simulation.

Thus, chemical association between the C atoms dissolved in the nanoparticle and the C atoms in the cap rim was not observed. Nevertheless, the occurrence of such association has been reported for nanoparticles with higher C content, where the incorporation of diffusing C atoms from the bulk of the nanoparticle into the nanotube rim has been observed for longer simulation times in classical molecular dynamics[37]. Although the migration of C atoms from the inner octahedral positions to the subsurface of the nanoparticle was evident, segregation to the exterior of the nanoparticle was never observed. This lack of carbon nanostructure growing pattern is attributed to a C concentration below that corresponding to saturation of the nanoparticle; i.e., even though all the octahedral sites were occupied (as it would be in the case of carbide formation), the nanoparticle may still dissolve more C atoms adopting a non-carbide structure, as observed in classical MD simulations of the SWCNT growth[37,38,60] before it becomes saturated and C atoms are segregated to the surface. This suggests that a particle with the pure carbide structure wouldn't facilitate the precipitation of C atoms to the surface, because their Ni-C interaction
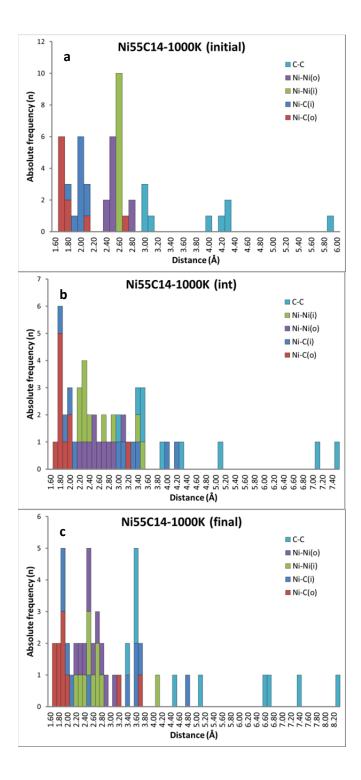
energies are too strong (Table 1). However, during SWCNT growth, the particle is under additional carbon pressure (not included in our simulations) that would facilitate saturation of the catalytic nanoparticle and subsequent carbon segregation to the surface and formation of carbon nanostructures.

Dynamics of the atomic pair interactions. Further insights can be obtained from the analysis of individual pairs of adjacent C atoms, Ni atoms, and Ni and C atoms that were randomly selected to be monitored throughout the simulation (Figure S1). The analysis reveals structural and chemical changes in the nanostructure of the carburized nanoparticles. A minimum of ten pairs of atoms for each pair type was considered in each simulation. The bars depicted in Figures 4a, b, and c represent the number of distances between pairs that fall within a specific range of distances ($\Delta d = 0.2$ Å). Figure 4a illustrates the behavior of the selected atom pairs in the carburized $Ni_{55}C_{14}$ nanoparticle at the beginning of the simulation, with C atoms located in octahedral sites at 1000 K. Distances between pairs of Ni atoms and Ni-C in the inner and outer layers of the nanoparticle show a narrow distribution, reflecting the initial state of order of the C atoms with respect to Ni and Ni within the original structure. The wider distribution of C-C distances arises from the fact that C atoms were initially located spread across the extension of the nanoparticle in octahedral positions. As the simulation progresses, the most significant changes observed in Figure 4b are the inner and outer distances of Ni-Ni pairs, which become wider as the Ni atoms in the nanoparticle fluctuate their position as a result of the high temperature dynamics. The distribution of C-C distances becomes even wider as some C atoms begin migrating towards the subsurface. Evidence of this C migration process is also observed from the inner Ni-C distribution becoming considerably flatter and wider than other distributions, thus indicating changes in the nanoparticle internal structure and the relative position of C atoms inside the Ni cluster. In contrast, the overall dynamic effects on the outer Ni and C atoms are balanced in such a way that the outer Ni-C distances maintain a narrow distribution approximately in the same range.

Figure 4 c shows the distribution of pair distances after 8 ps of simulation. At this point the nanoparticle structure is closer to an equilibrium state evidenced by narrower distributions of Ni-Ni and Ni-C with defined peaks located at 2.5- and 1.9-Å, respectively. Although the C-C distribution is wider here than at an intermediate stage, the presence of a peak at 3.6 Å indicates a relative ordering of the C atoms to some extent after migrating from their initial octahedral location to the subsurface. These results are in conformity with the pair radial distribution function (RDF) of all pairs of atoms in the nanoparticle with peaks located at 2.45-, 1.85-, and 3.45-Å for Ni-Ni, Ni-C and C-C respectively and comparable relative width (Figure S2 in Supporting Information).
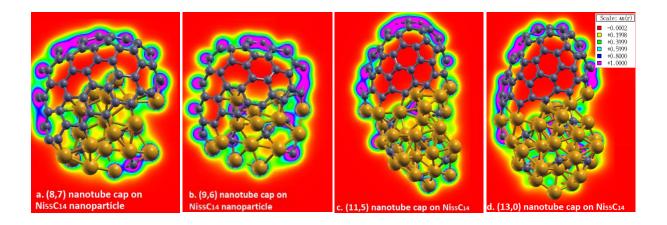
An increment in the width of the distribution of C-C peaks is observed for the nanoparticles with higher C content due to an increased driving force for the migration of the C atoms dissolved in the nanoparticle toward the subsurface. At low temperature the distribution of Ni-Ni and Ni-C distances tends to be narrower for the nanoparticles with higher C content as the arrangement of

atoms is more structured, whereas the opposite occurs at higher temperature where the dynamics plays a more important role in the relative motion of the atoms in the nanoparticle. Estimation of the C diffusion coefficients supports these ideas, as the motion is increased with increasing temperature and increasing carbon content (Table S1 in the supplementary information). In turn, a reduction in the sharpness of the C-C peaks is observed for the nanoparticles with lower C content. In all cases, the differences between inner and outer Ni-C and Ni-Ni distances are insignificant.

Figure 4. Histograms indicating the absolute frequency of atom pairs separated by a specific distance in the $Ni_{55}C_{14}$ carburized nanoparticle at 1000 K at a given simulation time: a) initial ~ 0 ps b) intermediate ~ 4 ps and c) final ~ 8 ps. Bar color code: C-C (blue), Ni-Ni(o) (purple), Ni-Ni(i) (green), Ni-C(i) (blue) and Ni-C(o) (red). The legend in parenthesis indicates whether the atoms were initially located at the nanoparticle surface (o) or the interior of the nanoparticle (i).

Nanoparticle morphology. Small changes in the overall shape of the nanoparticle are observed throughout the simulation. The unsupported carburized nanoparticles maintained a spherical shape characterized by the absence of stable, well-defined facets as the positions of the surface atoms presented small fluctuations due to the temperature-induced dynamics (Figure S1). Typical catalysts used in the synthesis of single walled carbon nanotubes that may exhibit well-defined facets have been reported[34]. Such structural features of the catalyst are believed to play an important role in the adsorption and lift off of the nascent nanotube cap. A significant factor that influences shape in real catalysts is the presence of a substrate, which depending on the strength of the metal-support interaction, may exhibit a more defined structure and thus may have a significant influence on the nanotube structure (template effect)[29,30,38,61]. In our model systems, the absence of a substrate leads to a moldable structure of the nanoparticle that can accommodate to the growing nanotube shape. This effect is known as inverse template effect[30] and can be observed in Figure 5. Round caps such as those of (8,7) and (9,6) help maintain a spherical shape in the nanoparticle; narrower and more elongated caps such as those of (11,5) and (13,0) cause the nanoparticle to adapt its shape to match more closely the shape of the nascent nanotube (Figures 5c and d). Similar reshaping effects have been observed from ETEM studies of SWCNT tip growth, a mode of growth in which the nanoparticle detaches from the substrate and remains attached to the nanotube tip, allowing greater mobility of the metal atoms and accommodation of the nanoparticle to the nanotube structure via capillary-driven surface diffusion[56].

Figure 5. Electron density maps for the carburized nanoparticle with a cap of chiral indexes a. (8,7), b. (9,6), c. (11,5), and d. (13,0). The color images were obtained using the software XCrySDen[62].

Electronic distribution. Changes in the electronic structure of the different nanoparticles considered in this study are examined by estimating partial atomic charges and charge
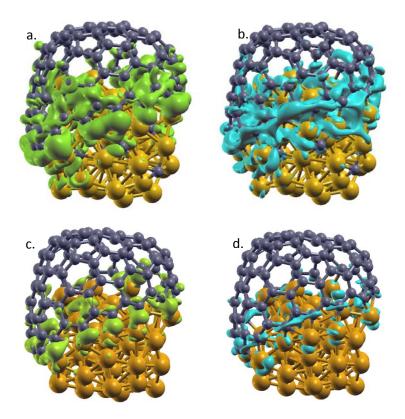
differences using a grid-based Bader analysis algorithm[48], plotting electron density maps, and calculating the electron density of states. The distribution of charges between Ni and C atoms in the carburized nanoparticle is slightly shifted with increasing carbon content and is not affected by changes in temperature. The average magnitude of the Ni and C atomic charges are +0.12 e and -0.68 e respectively for $Ni_{55}C_{10}$, whereas for $Ni_{55}C_{14}$ the Ni and C average charges are +0.18 e and -0.69 e respectively. Thus, the addition of C atoms to the carburized nanoparticle causes a stronger attraction between Ni and C evidenced by a slight increase in the magnitude of the average charges in both cases. This may also be a contributing factor to the wider distributions observed for the Ni-Ni and C-C distances in $Ni_{55}C_{14}$.

The electron density of the nanoparticles with and without model nanotube caps, after 3 and 8 ps of AIMD respectively, was mapped on planes parallel to the z direction. These planes were located to intersect rich regions of electron density in the nanoparticle and bonding between the nanotube C atoms as illustrated in Figure 5. The regions in red indicate the absence of electron density. The space around the nanoparticle is devoid of electron density showing that the size of the simulation box is sufficiently large to prevent interactions with periodic images. The electron density is localized around the closest contacts between C atoms in the nanotube cap and the Ni atoms at the nanoparticle surface, where catalyzed addition of C to atoms to the nanotube rim occurs. In all cases, high population of electron density is concentrated around C atoms both in the nanoparticle and the nanotube cap with electron densities of around 1 e/Å³(pink regions), whereas an intermediate electron density population is found around Ni atoms (green regions). This suggests the occurrence of interactions involving charge transfer between Ni and C atoms, as revealed by their respective charges. Similar results have been reported in previous studies with pure Ni_{55} clusters indicating an electronic charge transfer from Ni atoms to C atoms at the nanotube edge[36]. In order to visualize and describe such interactions, further calculations of charge differences were performed for the nanoparticle with nanotube caps (combined system) and each individual component of the system (nanoparticle and nanotube cap); they are discussed in the next section.
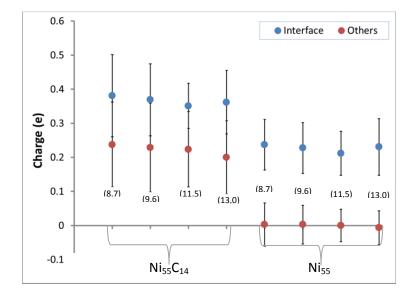
To further understand the role of C atoms dissolved in the nanocatalyst structure, an estimation of the energy of adhesion of the nanotube cap to the nanoparticle was performed on both pure Ni_{55} and the $Ni_{55}C_{14}$ carbide nanoparticles in contact with the four model nanotube caps, after running in AIMD for a time sufficiently long to reach equilibration. The energy of adhesion (depicted in Fig. S3) per carbon atom at the nanotube rim is fairly similar between metal and carbide nanoparticles. The maximum difference between energy of adhesion for a particular nanotube cap is 0.14 eV/C atom and no apparent preference for the nanotube models studied to attach to either nanoparticle were found.

Reactivity of the nanoparticle. Regions of electron accumulation and depletion were calculated for the four nanotube caps in contact with the $Ni_{55}C_{14}$ nanoparticle to display an isosurface with an isovalue of 0.03 e/Å³. Figures 6a and 6b illustrate the accumulation and depletion of electron density as result of the interaction between the carburized nanoparticle $Ni_{55}C_{14}$ and the nanotube

cap of indexes (9,6). Regions of electron accumulation are mainly localized at the space between the C atoms of the nanotube cap rim and the surface Ni atoms in direct contact with them.

Figure 6. Charge density difference analysis for $Ni_{55}C_{14}$ (a and b) and Ni_{55} (c and d) nanoparticles in contact with a nanotube cap with chiral indexes (9,6). Green regions in a and c correspond to electron accumulation. Blue regions in b and d correspond to electron depletion.

13

Figure 7. Average partial atomic charges for Ni atoms in $Ni_{55}C_{14}$ and Ni_{55} placed in contact with nanotube caps. Distinction is made between Ni atoms at the surface in contact with the cap (blue) and the remainder of Ni atoms (red).

This region of confined electron density provides an adequate reactive environment for the continuous incorporation of C atoms from the precursor environment in a typical CVD scheme. [63,64] Other regions of electron accumulation are located at the hexagons closest to the nanotube rim which may provide an environment that allows bond flexibility in the growing carbon lattice. This reasoning is consistent with previous observations indicating that C atoms in the vicinity of the rim are able to relocate within the nanotube network allowing the healing of defects[65]. Regions of electron depletion are mainly located in two types of regions: 1. Ni atoms in close contact with the nanotube cap. 2. Around C-C bonds located at the nanotube rim. This suggests that once C atoms have been incorporated into the nanotube rim, they partially donate their electron "share" to their neighbor Ni and C atoms in the vicinity of the rim, thus contributing to the reactivity of the nanotube-nanoparticle interface region and flexibility of the nanotube lattice near the cap rim. [64]

The accumulation and depletion of electron density as result of the interaction between the Ni_{55} nanoparticle and the nanotube cap of indexes (9,6) is depicted in Figures 7c and 7d. Regions of electron accumulation and depletion are located analogously in the metallic cluster Ni_{55} as in the carburized nanoparticle $Ni_{55}C_{14}$, however the degree of accumulation or depletion of electron density is notoriously larger in the carburized nanoparticle. The smaller individual regions of accumulation between the Ni surface atoms and the C atoms of the cap rim observed in Ni_{55} appear as a larger and more continuous region extended along the nanotube rim for $Ni_{55}C_{14}$. Similarly, disconnected depletion regions in the former appear merged in the latter. The implications of this observation may be significant in terms of reactivity, as electron rich environments are known to provide favorable conditions for sustained catalytic activity[66]. The presence of dissolved C atoms affects the electronic structure in the catalytic nanoparticle, increasing the strength of its interaction with the nascent nanotube and leading to larger electron accumulation and depletion regions. Evidence for the differences in the electronic structure of the two types of nanoparticles is found from the charge analysis of Bader and electron density of states. The density of states of Ni_{55} exhibits a population of electronic states concentrated in a smaller range of energies, and a lower density of unoccupied states above the Fermi level than $Ni_{55}C_{14}$, which is in agreement with electron accumulation and depletion diagrams and may be indicative of a higher reactivity of the $Ni_{55}C_{14}$ nanoparticle. Figure S4 shows a comparison of DOS for both nanoparticles in contact with the (8,7) cap. The analysis of charges summarized in Figure 7 also suggests a difference between the electronic structures of the two nanoparticles. Each Ni atom in both nanoparticles was classified as either "interface", if the atom was in direct contact with the nanotube rim, or "other" if it was located anywhere else. Regardless of the type of cap, all interfacial Ni atoms had an average partial charge of 0.4e⁻ for the carburized nanoparticle whereas the same for the metal nanoparticle was close to around 0.2e⁻. Other

internal and peripheral Ni atoms had an average close to 0.23e⁻ for the first case, whereas for the second it was close to 0.0e⁻. Thus, the presence of C atoms in the nanoparticle affects also Ni atoms not interacting directly with the rim, which may be exposed at the surface and may also contribute to the catalysis by virtue of a partial charge as opposed to being neutral as in the case of the pure Ni_{55}. It is worth mentioning that caps with different chiral indexes behaved in a similar fashion concerning the electronic structure description presented above.

Conclusions

The dynamic evolution of unsupported carburized Ni nanoparticles during the pre-growth and growth stages of single-walled carbon nanotubes was studied using density functional theory and ab initio molecular dynamics simulations. Carbon dissolution and stability of the carburized metal nanoparticle are observed throughout the simulation. Structural changes in the nanocatalyst structure are monitored through the extension of the simulation showing that in the absence of a substrate, the nanocatalyst fails to maintain a defined faceted structure. However, in the presence of a nascent nanotube cap, the floating catalyst accommodates to the shape of the nanotube shape in accordance with what is known as an "inverse template effect"[30]. The lack of association of carbon atoms inside the nanoparticle and evidence of short-range ordering from distance- and radial distribution function analyses may be indicators of the stability and potential for evolution of the nanoparticle system into a more thermodynamically stable phase such as that of a carbide phase. Moreover, lack of incorporation of C atoms from the nanoparticle into the nanotube rim may support the idea that a state of saturation or supersaturation of the nanoparticle is needed for precipitation of C from the stable Ni-C core to the surface, and incorporation to the nanotube rim to occur, leaving the most of the catalytic growth to the surface-diffusing C species as reported in previous studies[37]. Analyses of the electronic structure of the nanoparticle during growth reveal that a charge transfer process occurs from the surface Ni atoms and rim C atoms to the interfacial region between the growing nanotube and the nanoparticle. This process leaves an interfacial region rich in electron density, where incorporation of precursor C may continue the growth process, and electron-depleted regions in the vicinity of the nanotube rim that may allow rearrangement of the C atoms near the rim and healing of defects. A comparison between the charge transfer in a carburized nanoparticle and a pure metal nanoparticle reveals that the process occurs similarly in both systems, but in the case of the carburized nanoparticle the interfacial region is larger and almost continuous along the nanotube rim, whereas the metal nanoparticle displays a smaller and more localized accumulation region. Surface Ni atoms that are not in direct contact with the cap are also affected: a neutral charge characterizes surface Ni atoms in the pure nanoparticle, and positively charged Ni atoms are found at the carburized nanoparticle surface. These observations suggest that the carburized nanoparticle may be able to offer a more reactive environment for nanotube growth than the metallic one. Altogether, continued exploration of the structural and electronic characteristics of the nanocatalyst and its interactions with the growing nanotube in SWCNT synthesis may contribute with valuable insight that will eventually allow us to control the structure and properties of SWCNT.

Acknowledgements

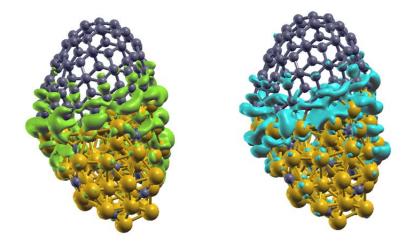## References

(1)   Jourdain, V.; Bichara, C.: *Carbon* 2013, **58**, 2-39.

(2)   Cao, Q.; Rogers, J. A.: *Advanced Materials* 2009, **21**, 29-53.

(3)   Kam, N. W. S.; O'Connell, M.; Wisdom, J. A.; Dai, H.: *Proceedings of the National Academy of Sciences of the United States of America* 2005, **102**, 11600-11605.

(4)   López-Lorente, A. I.; Simonet, B. M.; Valcárcel, M.: *Analytical Chemistry* 2010, **82**, 5399-5407.

(5)   An, K. H.; Kim, W. S.; Park, Y. S.; Moon, J.-M.; Bae, D. J.; Lim, S. C.; Lee, Y. S.; Lee, Y. H.: *Advanced functional materials* 2001, **11**, 387-392.

(6)   De Volder, M. F. L.; Tawfick, S. H.; Baughman, R. H.; Hart, A. J.: *Science* 2013, **339**, 535-539.

(7)   Tans, S. J.; Verschueren, A. R. M.; Dekker, C.: *Nature* 1998, **393**, 49-52.

(8)   Srivastava, N.; Banerjee, K.: Performance analysis of carbon nanotube interconnects for VLSI applications. In *Computer-Aided Design, 2005. ICCAD-2005. IEEE/ACM International Conference on*, 2005; pp 383-390.

(9)   Britto, P. J.; Santhanam, K. S.; Rubio, A.; Alonso, J. A.; Ajayan, P. M.: *Advanced Materials* 1999, **11**, 154-157.

(10)   Bachilo, S. M.; Strano, M. S.; Kittrell, C.; Hauge, R. H.; Smalley, R. E.; Weisman, R. B.: *Science* 2002, **298**, 2361-2366.

(11)   Treacy, M. M. J.; Ebbesen, T. W.; Gibson, J. M.: *Nature* 1996, **381**, 678-680.

(12)   Prasek, J.; Drbohlavova, J.; Chomoucka, J.; Hubalek, J.; Jasek, O.; Adam, V.; Kizek, R.: *Journal of Materials Chemistry* 2011, **21**, 15872-15884.

(13)   Dresselhaus, M. S.; Dresselhaus, G.; Eklund, P. C.: *Science of fullerenes and carbon nanotubes: their properties and applications*; Academic press, 1996.

(14)   Arnold, M. S.; Green, A. A.; Hulvat, J. F.; Stupp, S. I.; Hersam, M. C.: *Nat Nano* 2006, **1**, 60-65.

(15)   Liu, H.; Nishide, D.; Tanaka, T.; Kataura, H.: *Nature communications* 2011, **2**, 309.

(16)   Chng, E. L. K.; Poh, H. L.; Sofer, Z.; Pumera, M.: *Phys. Chem. Chem. Phys.* 2013, **15**, 5615-5619.

(17)   Kong, J.; Cassell, A. M.; Dai, H.: *Chemical Physics Letters* 1998, **292**, 567-574.

(18)   Alvarez, W. E.; Pompeo, F.; Herrera, J. E.; Balzano, L.; Resasco, D. E.: *Chemistry of Materials* 2002, **14**, 1853-1858.

(19)   Li, Y.; Kim, W.; Zhang, Y.; Rolandi, M.; Wang, D.; Dai, H.: *The Journal of Physical Chemistry B* 2001, **105**, 11424-11431.

(20)   Huang, S.; Woodson, M.; Smalley, R.; Liu, J.: *Nano Letters* 2004, **4**, 1025-1028.

(21)   Page, A. J.; Ohta, Y.; Irle, S.; Morokuma, K.: *Accounts of chemical research* 2010, **43**, 1375-1385.

(22)   Amara, H.; Bichara, C.; Ducastelle, F.: *Physical review letters* 2008, **100**, 056105.

(23)   Gomez-Gualdron, D. A.; McKenzie, G. D.; Alvarado, J. F.; Balbuena, P. B.: *ACS nano* 2011, **6**, 720-735.

(24)   Zhu, H.; Suenaga, K.; Wei, J.; Wang, K.; Wu, D.: *Journal of Crystal Growth* 2008, **310**, 5473-5476.

(25)   Oberlin, A.; Endo, M.; Koyama, T.: *Journal of Crystal Growth* 1976, **32**, 335-349.

(26)   Audier, M.; Oberlin, A.; Coulon, M.: *Journal of Crystal Growth* 1981, **55**, 549-556.

(27)   Hofmann, S.; Sharma, R.; Ducati, C.; Du, G.; Mattevi, C.; Cepek, C.; Cantoro, M.; Pisana, S.; Parvez, A.; Cervantes-Sodi, F.; Ferrari, A. C.; Dunin-Borkowski, R.; Lizzit, S.; Petaccia, L.; Goldoni, A.; Robertson, J.: *Nano Letters* 2007, **7**, 602-608.

(28)   Reich, S.; Li, L.; Robertson, J.: *Chemical physics letters* 2006, **421**, 469-472.

(29)   Koziol, K. K.; Ducati, C.; Windle, A. H.: *Chemistry of Materials* 2010, **22**, 4904-4911.

(30)   Gómez-Gualdrón, D. A.; Zhao, J.; Balbuena, P. B.: *The Journal of Chemical Physics* 2011, **134**, -.

(31)   Cheng, H. M.; Li, F.; Su, G.; Pan, H. Y.; He, L. L.; Sun, X.; Dresselhaus, M. S.: *Applied Physics Letters* 1998, **72**, 3282-3284.

(32)   Ci, L.; Wei, J.; Wei, B.; Liang, J.; Xu, C.; Wu, D.: *Carbon* 2001, **39**, 329-335.

(33)   Fan, Y.-Y.; Kaufmann, A.; Mukasyan, A.; Varma, A.: *Carbon* 2006, **44**, 2160-2170.

(34)   Picher, M.; Lin, P. A.; Gomez-Ballesteros, J. L.; Balbuena, P. B.; Sharma, R.: *Nano letters* 2014, **14**, 6104-6108.

(35)   Börjesson, A.; Bolton, K.: *The Journal of Physical Chemistry C* 2010, **114**, 18045-18050.

(36)   Wang, Q.; Yang, S.-W.; Yang, Y.; Chan-Park, M. B.; Chen, Y.: *The Journal of Physical Chemistry Letters* 2011, **2**, 1009-1014.

(37)   Gómez-Gualdrón, D. A.; Balbuena, P. B.: *Carbon* 2013, **57**, 298-309.

(38)   Gómez-Gualdrón, D. A.; Beetge, J. M.; Balbuena, P. B.: *The Journal of Physical Chemistry C* 2013, **117**, 12061-12070.

(39)   Perdew, J. P.; Burke, K.; Ernzerhof, M.: *Physical review letters* 1996, **77**, 3865.

(40)   Kresse, G.; Furthmüller, J.: *Physical Review B* 1996, **54**, 11169.

(41)   Kresse, G.; Furthmüller, J.: *Computational Materials Science* 1996, **6**, 15-50.

(42)   Kresse, G.; Hafner, J.: *Physical Review B* 1993, **47**, 558.

(43)   Kresse, G.; Hafner, J.: *Physical Review B* 1993, **48**, 13115.

(44)   Kresse, G.; Hafner, J.: *Physical Review B* 1994, **49**, 14251.

(45)   Blöchl, P. E.: *Physical Review B* 1994, **50**, 17953.

(46)   Kresse, G.; Joubert, D.: *Physical Review B* 1999, **59**, 1758.

(47)   Henkelman, G.; Arnaldsson, A.; Jónsson, H.: *Computational Materials Science* 2006, **36**, 354-360.

(48)   Tang, W.; Sanville, E.; Henkelman, G.: *Journal of Physics: Condensed Matter* 2009, **21**, 084204.

(49)   Inc., A. S.: *San Diego: Accelrys Software Inc.* 2013.

(50)   Brinkmann, G.; Friedrichs, O. D.; Lisken, S.; Peeters, A.; Van Cleemput, N.: *MATCH Commun. Math. Comput. Chem* 2010, **63**, 533-552.

(51)   Reich, S.; Li, L.; Robertson, J.: *Physical Review B* 2005, **72**, 165423.

(52)   Diarra, M.; Amara, H.; Ducastelle, F.; Bichara, C.: *physica status solidi (b)* 2012, **249**, 2629-2634.

(53)   Diarra, M.; Zappelli, A.; Amara, H.; Ducastelle, F.; Bichara, C.: *Physical Review Letters* 2012, **109**, 185501.

(54)   Ding, F.; Bolton, K.; Rosén, A.: *Journal of Vacuum Science & Technology A* 2004, **22**, 1471-1476.

(55)   Yoshida, H.; Takeda, S.; Uchiyama, T.; Kohno, H.; Homma, Y.: *Nano Lett.* 2008, **8**, 2082-2086.

(56)   Moseler, M.; Cervantes-Sodi, F.; Hofmann, S.; Csányi, G.; Ferrari, A. C.: *ACS Nano* 2010, **4**, 7587-7595.

(57)   Ni, L.; Kuroda, K.; Zhou, L.-P.; Ohta, K.; Matsuishi, K.; Nakamura, J.: *Carbon* 2009, **47**, 3054-3062.

(58)   Nagakura, S.: *Journal of the Physical Society of Japan* 1957, **12**, 482-494.

(59)   Nagakura, S.: *Journal of the Physical Society of Japan* 1958, **13**, 1005-1014.

(60)   Page, A. J.; Yamane, H.; Ohta, Y.; Irle, S.; Morokuma, K.: *Journal of the American Chemical Society* 2010, **132**, 15699-15707.

(61)   Jiang, A.; Awasthi, N.; Kolmogorov, A. N.; Setyawan, W.; Börjesson, A.; Bolton, K.; Harutyunyan, A. R.; Curtarolo, S.: *Physical Review B* 2007, **75**, 205426.

(62)   Kokalj, A.: *Computational Materials Science* 2003, **28**, 155-168.

(63)   Gomez-Gualdron, D. A.; Balbuena, P. B.: *J. Phys. Chem. C* 2009, **113**, 698-709.

(64)   Gomez-Gualdron, D. A.; Balbuena, P. B.: *Nanotechnology* 2009, **20**, 215601.

(65)   Burgos, J. C.; Jones, E.; Balbuena, P. B.: *The Journal of Physical Chemistry C* 2014, **118**, 4808-4817.

(66)   Martínez de la Hoz, J. M.; Balbuena, P. B.: *The Journal of Physical Chemistry C* 2011, **115**, 21324-21333.

Table of Contents Figure

Carburized Ni nanoparticle/carbon cap shows electron accumulation (green) at the metal/rim interface and depletion (blue) on the rim C-C bonds.